On the Stability of $IrCl_6^{3-}$ and Other Triply Charged Anions: Solvent Stabilization versus Ionic Fragmentation and Electron Detachment for the $IrCl_6^{3-}\cdot(H_2O)_n$ $n = 0-10$ Microsolvated Clusters

William E. Boxford and Caroline E. H. Dessent*

Department of Chemistry, University of York, Heslington, York, YO10 5DD, U.K.

Received: January 28, 2005; In Final Form: April 14, 2005

The intrinsic gas-phase stability of the $IrCl_6^{3-}$ trianion and its microsolvated clusters, $IrCl_6^{3-}\cdot(H_2O)_n$ $n = 1-10$, have been investigated using density functional theory (DFT) calculations. Although $IrCl_6^{3-}$ is known to exist as a stable complex ion in bulk solutions, our calculations indicate that the bare trianion is metastable with respect to decay via both electron detachment and ionic fragmentation. To estimate the lifetime of $IrCl_6^{3-}$, we have computed the electron tunneling probability using an adaption of the Wentzel−Kramer−Brillouin theory and predict that the trianion will decay spontaneously via electron tunneling on a time scale of 2.4×10^{-13} s. The global minimum structure for $IrCl_6^{3-}\cdot H_2O$ was found to contain a bifurcated hydrogen bond, whereas for $IrCl_6^{3-}\cdot(H_2O)_2$, two low energy minima were identified; one involving two bifurcated water-ion hydrogen bonds and a second combining a bifurcated hydrogen bond with a water−water hydrogen bond. Clusters based on each of these structural motifs were obtained for all of the $n = 3-10$ systems, and the effect of solvation on the possible decay pathways was explored. The calculations reveal that solvation stabilizes $IrCl_6^{3-}$ with respect to *both* electron detachment decay and ionic fragmentation, with the magnitude of the repulsive Coulomb barrier for ionic fragmentation increasing smoothly with sequential solvation. This study is the first to compare the propensity for electron detachment versus ionic fragmentation decay for a sequentially solvated triply charged anion.

1. Introduction

There has been considerable recent interest in the intrinsic properties of gas-phase multiply charged anions (MCAs) because of experimental developments that allow their detailed characterization using laser spectroscopy.[1] MCAs represent highly energetic species in the gas phase because of the strength of the repulsive Coulomb interaction in the absence of a moderating dielectric environment.[2−5] As a result, isolated MCAs are highly susceptible to decay via electron detachment[3,6−7] or through fragmentation into two ionic moieties (i.e., thermodynamic decay).[4,8,9] This leads to a situation in which small unsolvated molecular MCAs are frequently either entirely unstable or subject to rapid unimolecular decay.

Although multiply charged ions can be regarded as exotic, metastable species in the gas-phase, they are common components of polar solutions and ionic solids. Within a condensed phase environment, the solvent acts to stabilize excess charge and reduces the extent of the Coulombic repulsion via dielectric screening. It is therefore of fundamental interest to question how an isolated multiply charged ion is solvated and stabilized. The microsolvation of multiply charged metal cations, $[M(Sol)_n]^{z+}$, has already been the focus of a number of experiments in which small clusters have been investigated to model the transition from the gas phase to the condensed phase limit.[10−13] Cluster studies exploring the sequential solvation of MCAs, however, are sparse in comparison. Although a small number of studies have focused on the solvation of molecular dianions (e.g., dicarboxylate dianions and SO_4^{2-}),[14−20] the microsolvation of triply or quadruply charged molecular anions has been largely ignored.[21]

Previous experimental and theoretical studies of molecular dianions have illustrated that the propensity for electron detachment decreases smoothly with the sequential addition of water molecules.[14−18] A similar trend is expected for more highly charged anions. We are therefore particularly interested in the issue of how water complexation affects the stability of an MCA with respect to ionic fragmentation. Harvey and Kaczorowska have recently investigated the effect of microsolvation on highly charged metal cations such as Zr^{4+}.[13] Intriguingly, they found that although Zr^{4+} was stabilized by sequential solvation with 1−6 water molecules, addition of a seventh water molecule in the second solvation shell led to spontaneous dissociation of the system via ionic fragmentation into H_3O^+ and $[ZrOH(H_2O)_5]^{3+}$. If similar effects occurred for anions, then it would have important practical consequences for the preparation of isolated, metastable MCAs because the most general method for their preparation, electrospray ionization, involves the generation of bare gas-phase ions via evaporation of microdroplets from a bulk solution.

In this paper, we investigate the intrinsic gas-phase stability of the $IrCl_6^{3-}$ trianion using primarily density functional theory (DFT) calculations. To estimate the lifetime of $IrCl_6^{3-}$ with respect to electron detachment, that is

$$IrCl_6^{3-} \rightarrow IrCl_6^{2-} + e^- \qquad (1)$$

we have calculated a potential surface using the "point charge" model of Dreuw and Cederbaum,[22] and applied Wentzel−Kramer−Brillouin theory to estimate the tunneling lifetime. $IrCl_6^{3-}$ can also be unstable with respect to decay via ionic fragmentation, that is

* Corresponding author. Fax: 44-1904-432516. E-mail: ced5@york.ac.uk.

10.1021/jp0505025 CCC: $30.25
Published on Web 06/15/2005

$$IrCl_6^{3-} \rightarrow IrCl_5^{2-} + Cl^- \quad (2)$$

We present calculations investigating the sequential solvation of $IrCl_6^{3-}$ to investigate how the electronic and thermodynamic stability of $IrCl_6^{3-}$ is moderated by the effect of solvation. The $IrCl_6^{3-}$ system was chosen as a prototype because the doubly charged $IrCl_6^{2-}$ and $IrBr_6^{2-}$ ions have been studied experimentally using both photodetachment and photofragmentation spectroscopy,[23,24] providing important benchmarks for the calculations performed. This study is the first to compare the propensity for electron detachment versus ionic fragmentation decay for a sequentially solvated triply charged anion.

Octahedral or quasioctahedral hexahalogenometalate trianions such as $IrCl_6^{3-}$ are classical Werner-type transition-metal complexes[25] and are commonly found as constituents of solids, melts, and solutions. These species are of interest as electron transfer agents in solution, and have been studied extensively as such.[26] There is no gas-phase work on these species to date, and it is unknown if they are stable as free trianions and can be formed in the gas phase.

2. Computational Methods

The equilibrium geometries, energies, and harmonic vibrational frequencies of the ions and clusters studied in this work were calculated with the B3LYP hybrid exchange and correlation functional[27] and the LANL2DZ basis (Los Alamos ECP on the metal core with the associated double-ζ basis on the valence electrons) on all atoms.[28] In addition, selective single point calculations were performed at the MP2 level of theory for comparison with the DFT results. All of the calculations were carried out using GAUSSIAN 03,[29] with the default convergence criteria applied to the geometry optimizations. Partial charge distributions were calculated using the natural population analysis (NPA) method.[30]

Vertical detachment energies (VDEs) were calculated as the difference between the total energy of the MCA and the corresponding detached anion at the optimized geometry of the MCA. Adiabatic detachment energies (ADEs) were calculated as the difference between the total energies of the optimized structures of the MCA and the corresponding detached anion. Zero point energy (ZPE)-corrected ADEs were also computed by adding the harmonic ZPE (unscaled) to the respective total energies of the MCA and the detachment product.

DFT (B3LYP) has been chosen as the preferred methodology for this study primarily on the grounds of computational economy because the solvated molecular clusters under study are relatively large. In general, B3LYP has been found to reproduce the geometric structures of hydrogen bonding systems reliably.[31,32] The solvation of singly charged anions (e.g., $Cl^-\cdot(H_2O)_n$ clusters) has been studied intensively in recent years,[33−39] with detailed experiments providing a robust test of computational methods. DFT (using the B3LYP functional) has been employed widely by experimental groups working in this area to interpret their data[33−35] and has proved to be highly reliable in terms of predicting cluster structures and vibrational frequencies. These DFT results are generally in excellent agreement with additional theoretical studies that have employed MP2 calculations.[36−38] Given that similar noncovalent interactions occur in systems such as $Cl^-\cdot(H_2O)_n$, and $IrCl_6^{3-}\cdot(H_2O)_n$, DFT should therefore prove to be an appropriate methodology for this work.

3. Results and Discussion

A. The Stability of $IrCl_6^{2-}$ and $IrBr_6^{2-}$ with Respect to Electron Detachment and Ionic Fragmentation. Figure 1a displays the optimized structure of the $IrCl_6^{2-}$ dianion obtained at the B3LYP/LANL2DZ level. The D_{4h} geometry results from Jahn−Teller distortion away from the higher symmetry O_h structure because of the d^5 electronic configuration. Bond lengths and atomic partial charges are included on the figure. The $IrCl_6^{2-}$ bond lengths obtained agree well with the experimental crystallographic value[40] (average bond length = 2.47 Å), and the calculated geometric structure agrees well with a previous calculation.[41]

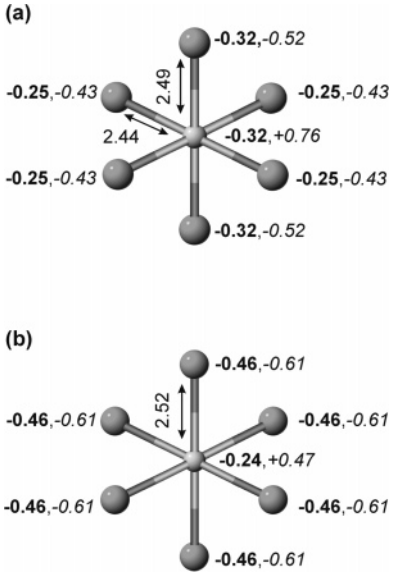

Figure 1. Geometric structures (B3LYP/LANL2DZ) of the optimized global minima of (a) the $IrCl_6^{2-}$ dianion and (b) the $IrCl_6^{3-}$ trianion. Bond lengths are in Angstroms, Mulliken charges are in bold, and NPA charges are in italics.

The VDEs and ADEs of $IrCl_6^{2-}$ are presented in Table 1, along with values for the related $IrBr_6^{2-}$ dianion. The VDEs and ADEs obtained are generally in good qualitative agreement with the experimental values.[23] We emphasize that the positive VDEs and ADEs obtained indicate that $IrCl_6^{2-}$ and $IrBr_6^{2-}$ are energetically stable with respect to electron detachment, a result that is consistent with the fact that these species can be prepared as isolated gas-phase ions.[8,23,24]

The potential energy surfaces of MCAs are dominated by repulsive Coulomb barriers (RCB), features which arise from a combination of short-range attractive and long-range repulsive forces.[1−3] The point charge method of Dreuw and Cederbaum was applied to model the potential energy surface for electron detachment from $IrCl_6^{2-}$.[22] Figure 2a displays two 1D cuts along the electron detachment surface of $IrCl_6^{2-}$, with the maximum value of *V(r)* representing the RCB_{ed}(outer) height, that is, the barrier measured from the $IrCl_6^- + e^-$ asymptote. The point charge method describes the short-range interaction rather poorly so that the magnitude of RCB_{ed}(inner), that is, the barrier measured from the $IrCl_6^{2-}$ minimum, is more reliably obtained as the sum of RCB_{ed}(outer) and the ADE.[42] We note that the $IrCl_6^{2-}$ surface for electron detachment is anisotropic, with the minimum energy path lying along the axial bond axis (RCB_{ed}(inner) = 3.26 eV) and the maximum energy pathway lying between the bond axes (RCB_{ed}(inner) = 4.04 eV). Table 1 lists the results obtained for RCB_{ed} along the minimum energy pathway for both $IrCl_6^{2-}$ and $IrBr_6^{2-}$. The experimental and calculated values are generally in good qualitative agreement, particularly given that the RCB_{ed} values obtained using photoelectron spectroscopy are approximate.[1]

Calculations were also performed to investigate ionic fragmentation of the IrX_6^{2-} (X = Cl^-, Br^-) dianions. Table 1

TABLE 1: Calculated VDEs, ADEs, RCB Heights (eV), and Tunnelling Lifetimes (s) for Electron Detachment, Presented with Energetics and RCB Heights for Ionic Fragmentation for $IrCl_6^{2-}$, $IrBr_6^{2-}$, $IrCl_6^{3-}$, $RuCl_6^{3-}$, and $RhCl_6^{3-}$ and Compared with Experimental Results

	$IrCl_6^{2-}$		$IrBr_6^{2-}$		$IrCl_6^{3-}$	$RuCl_6^{3-}$	$RhCl_6^{3-}$
	calcd[a]	exptl[b]	calcd[a]	exptl[b]	calcd[a]	calcd[a]	calcd[a]
VDE	1.00	0.98 ± 0.05	0.92	1.09 ± 0.05	-3.88	-4.00	-3.29
ADE	0.92 (0.93)	0.82 ± 0.05	0.95 (0.94)	0.96 ± 0.06	-4.06 (-4.04)	-4.24 (-4.22)	-3.46 (-3.44)
RCB_{ed}(inner)	3.26[c]	~2.5	2.95[c]	≤3.0	1.28[c]	1.25	1.79
RCB_{ed}(outer)	2.34[c]	~1.7	2.00[c]	≤2.0	5.34[c]	5.49	5.25
lifetime[d]	∞		∞		2.4×10^{-13}	9.4×10^{-14}	3.0×10^{-10}
ΔE_{if}	-0.20 (-0.24)		-0.82 (-0.83)	-0.6 ± 0.4	-4.49	-5.00	-5.50
RCB_{if}(inner)	1.38		1.00	1.6 ± 0.2	0.58	0.33	0.46
RCB_{if}(outer)	1.58		1.82	2.2 ± 0.2	5.07	5.33	5.96

[a] Calculated at the B3LYP/LANL2DZ level. Zero point energy corrected values shown in parantheses. [b] References 23 and 24. [c] Calculated using the point charge model.[22] [d] Calculated using an adaptation of WKB theory.[22,42]

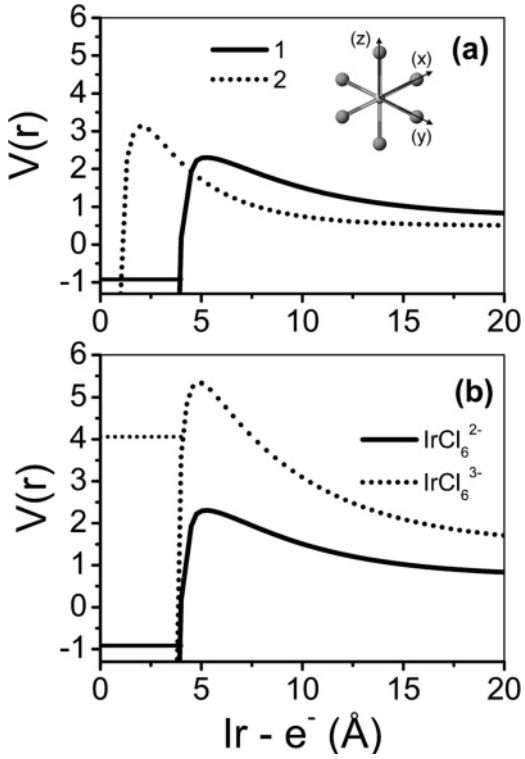

Figure 2. One-dimensional cuts through RCB_{ed} of $IrCl_6^{2-}$ and $IrCl_6^{3-}$, calculated using the point charge model (see text) at the B3LYP/LANL2DZ level. (a) Two cuts along RCB_{ed} of $IrCl_6^{2-}$. Potential 1 is a cut along the minimum energy path, which lies along an axial Ir−Cl bond (i.e., *z* axis in inset). Potential 2 is a cut along the maximum energy path, which lies equidistant between the bond axes. The horizontal line represents the energy of the $IrCl_6^{2-}$ global minimum. (b) Cuts through RCB_{ed} of $IrCl_6^{2-}$ and $IrCl_6^{3-}$ along the minimum energy path. Solid and dotted horizontal lines represent the energy of the $IrCl_6^{2-}$ and $IrCl_6^{3-}$ global minima, respectively.

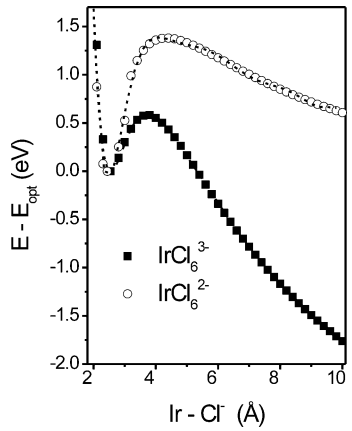

Figure 3. Calculated potential energy curves for the ionic fragmentation process of $IrCl_6^{n-} \rightarrow IrCl_5^{(n-1)-} + Cl^-$, $n = 2, 3$. The curves were obtained as a function of the axial Ir−Cl⁻ distance. All of the other geometric parameters were fully optimized at the B3LYP/LANL2DZ level.

presents values for the energetics (ΔE_{if}), illustrating that fragmentation is exothermic for both dianions. Fully relaxed scans were performed as a function of the Ir−X distance to model the potential energy surfaces and to investigate the nature of the repulsive Coulomb barrier for ionic fragmentation, RCB_{if}. Values for RCB_{if}(inner) and RCB_{if}(outer) are displayed in Table 1, with a potential energy surface displayed in Figure 3. (We define RCB_{if}(inner) and RCB_{if}(outer) as for the electron detachment potential energy surface so that RCB_{if}(inner) refers to the barrier height from the IrX_6^{2-} minimum and RCB_{if}(outer) refers to the barrier height from the $IrX_5^- + X^-$ asymptote.)

The calculated RCB_{if}(inner) and RCB_{if}(outer) for $IrBr_6^{2-}$ of 1.00 and 1.82 eV, respectively, are in reasonable agreement with the experimental values of 1.6 ± 0.2 and 2.2 ± 0.2 eV.[24] In comparing the computed and experimental values, we note that the experimental authors describe their quoted error as an "estimated error". Recent attempts to calculate a similar potential energy for the BeC_n^{2-} dianion at the MP2 level of theory failed to reproduce an RCB,[43] and the DFT results presented here can be viewed very favorably in this light. Although ΔE_{if} is exothermic for $IrCl_6^{2-}$ and $IrBr_6^{2-}$, the substantial RCB_{if}(inner) barriers render the dianions metastable with respect to ionic fragmentation because tunneling through the RCB will be extremely inefficient for the heavy halide ions. These results are again consistent with the fact that these species can be observed as isolated gas-phase ions.[8,23,24]

Overall, the very reasonable performance of the B3LYP/LANL2DZ combination against the available data for the gas-phase $IrCl_6^{2-}$ and $IrBr_6^{2-}$ dianions gives us confidence that our results will be more than accurate enough for the primarily qualitative purposes of this study of the related $IrCl_6^{3-}$ trianion.

B. Stability of the $IrCl_6^{3-}$ Trianion with Respect to Electron Detachment and Ionic Fragmentation. Figure 1b displays the optimized structure of the $IrCl_6^{3-}$ trianion. The O_h symmetry structure is consistent with the d^6 electronic configuration. As expected, the Ir−Cl bond lengths of the trianion are longer than those in $IrCl_6^{2-}$ because of the additional Coulombic repulsion present at the global minimum geometry. The calculated ADEs and VDEs for $IrCl_6^{3-}$ (Table 1) reveal that the trianion is electronically unstable with respect to electron loss, in sharp contrast to the corresponding dianion. The limited

basis set employed in the current calculations will certainly affect the accuracy of the calculated EAs, and the inclusion of diffuse functions would make the values calculated more positive. Dreuw and Cederbaum discuss this point explicitly in their recent study of the $N(BF_3)_4^{3-}$ trianion.[44]

Figure 2b displays the minimum energy pathway for electron detachment from $IrCl_6^{3-}$ compared to $IrCl_6^{2-}$. The RCB_{ed}(outer) is substantially larger for the trianion (5.34 eV) than for the dianion (2.34 eV), as expected because of the increased Coulombic repulsion present in the trianion. Conversely, RCB_{ed}(inner) becomes dramatically smaller on going from the dianion (3.26 eV) to the trianion (1.28 eV), an effect that arises because of the relatively weaker binding energy of an electron to the dianion compared to a monoanion.[15]

The asymptote for electron detachment lies above the global minimum for the $IrCl_6^{2-}$ and $IrBr_6^{2-}$ dianions, so detachment via tunneling from the ground-state cannot occur. For $IrCl_6^{3-}$, however, tunneling will occur because the asymptote for electron detachment lies far below the global minimum. To estimate the tunneling lifetime for $IrCl_6^{3-}$, we applied an adaptation of the Wentzel−Kramers−Brillouin (WKB) theory.[22,42] Using an exponential fit of the outer barrier along the minimum energy path (Figure 2b) to describe the potential, a lifetime of 2.4×10^{-13} s is obtained. (We note that this value must be considered an estimate because the accuracy of the WKB lifetime depends on the reliability of the electron affinity used in the calculation. As discussed above, the calculated EA of $IrCl_6^{3-}$ would become more positive upon inclusion of diffuse functions to the basis set,[44] leading to a longer lifetime. For example, if the inclusion of diffuse functions produced an EA of −3.5 eV, this would give a lifetime of 3.6×10^{-12} s. The extremely short lifetime indicates that electron detachment will occur on a time scale that is likely to be too fast for detection of $IrCl_6^{3-}$ using standard mass spectrometric techniques. Therefore, although RCB_{ed} confers limited electronic metastability on $IrCl_6^{3-}$, we predict that the bare trianion will decay rapidly to $IrCl_6^{2-}$.

To investigate the generality of the $IrCl_6^{3-}$ results, we repeated the calculations described above for the related $RuCl_6^{3-}$ and $RhCl_6^{3-}$ trianions. The VDEs, ADEs, RCBs, and tunneling lifetimes are presented in Table 1. Like $IrCl_6^{3-}$, the other trianions also possess negative ADEs leading to short tunneling lifetimes, indicating that these trianions will decay rapidly via electron detachment. We note that the tunneling lifetimes obtained for $IrCl_6^{3-}$, $RuCl_6^{3-}$, and $RhCl_6^{3-}$ are in line with a value of 9.4×10^{-14} s obtained previously for the PO_4^{3-} trianion.[42]

The potential energy surface for ionic fragmentation of $IrCl_6^{3-}$ was modeled following the approach applied to the dianions above. Values for RCB_{if}(inner) and RCB_{if}(outer) are again displayed in Table 1, along with values for $RuCl_6^{3-}$ and $RhCl_6^{3-}$. Figure 3 shows the calculated potential energy surface for ionic fragmentation of $IrCl_6^{3-}$ displayed with the surface for $IrCl_6^{2-}$ for comparison. The same trends as those on the related electron detachment surfaces are evident, that is, RCB_{if}(outer) for the trianion (5.07 eV) is considerably larger than for the dianion (1.58 eV), reflecting the increased intramolecular Coulombic repulsion present in the trianion, whereas RCB_{if}(inner) is significantly smaller for the trianion (0.58 eV) than the dianion (1.38 eV) because of the weaker purely attractive binding of a Cl^- ligand to $IrCl_5^{2-}$ compared to $IrCl_5^-$.[8] Unlike the electron detachment surface, however, the presence of RCB_{if} means that $IrCl_6^{3-}$ will be metastable with respect to ionic fragmentation because Cl^- is too heavy to tunnel through the RCB.

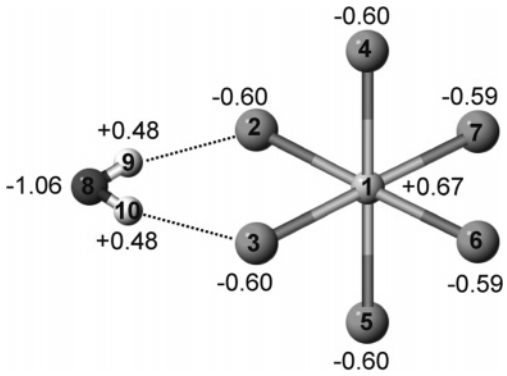

Figure 4. Geometric structure of the $IrCl_6^{3-}\cdot H_2O$ cluster obtained at the B3LYP/LANL2DZ level, displayed with NPA charges. Atom labels are in bold.

Finally, the 1D surface for ionic fragmentation corresponding to the simultaneous loss of two Cl^- ligands from $IrCl_6^{3-}$ was also investigated, that is,

$$IrCl_6^{3-} \rightarrow IrCl_4^- + 2Cl^- \qquad (3)$$

Pathway 3 was found to be more exothermic ($\Delta E_{if} = -5.89$ eV) than the loss of a single Cl^-, but the RCB_{if}(inner) was found to be far larger, displaying a height of 1.81 eV. Therefore, pathway 1 should represent the preferred lower energy ionic fragmentation pathway for $IrCl_6^{3-}$.

C. Microsolvation of the $IrCl_6^{3-}$ Trianion: Absolute Energies and Geometric Structures of the $IrCl_6^{3-}\cdot(H_2O)_n$ $n = 1-10$ Clusters. Although $IrCl_6^{3-}$ is known to be a stable complex anion in the condensed phase, the calculations presented in Section 4B indicate that the trianion is metastable with respect to ionic fragmentation and is prone to spontaneous decay via electron detachment. In this section, we present energies and geometric structures for the microsolvated $IrCl_6^{3-}\cdot(H_2O)_n$ $n = 1-10$ clusters. These structures will be used to explore the effect of solvation on the intrinsic stability of $IrCl_6^{3-}$ with respect to both ionic fragmentation and electron detachment in Section 3D.

(i) n = 1. Figure 4 displays the global minimum of the $IrCl_6^{3-}\cdot H_2O$ cluster obtained at the B3LYP/LANL2DZ level.

The absolute energy, water binding energy, VDE, and ADE for the complex are listed in Table 2, with geometric parameters in Table 3. Other cluster geometries subjected to optimization collapsed to the $IrCl_6^{3-}\cdot H_2O$ structure displayed. The minimum energy structure corresponds to a bifurcated hydrogen-bonding structure possessing C_{2v} symmetry (this binding mode will be referred to as motif a). Similar solvation motifs have been observed in previous ab initio work on dianion−water clusters such as $CO_2-(CH_2)_4-CO_2^{2-}\cdot H_2O$,[17] and $SO_4^{2-}\cdot H_2O$.[15,20] The NPA charges displayed on the figure indicate that a small amount of charge transfer occurs in the cluster, with −0.1e being transferred from the anion to the water.

(ii) n = 2. Figure 5 displays the six stable minima of the $IrCl_6^{3-}\cdot(H_2O)_2$ cluster obtained at the B3LYP/LANL2DZ level. The absolute energies, relative energies, VDEs, and ADEs are presented in Table 2, with geometric parameters listed in Table 3. The NPA charges are displayed on the Figure.

The structures and energies of the $IrCl_6^{3-}\cdot(H_2O)_2$ clusters are determined by the relative strengths of the pairwise ion−solvent and intersolvent interactions. Cluster I, the lowest energy structure, corresponds to a C_s symmetry structure in which one water molecule adopts a symmetric bifurcated hydrogen bond with respect to $IrCl_6^{3-}$ and acts as an acceptor to form a

TABLE 2: B3LYP/LANL2DZ Absolute Energies, Vertical Detachment Energies (VDE), Adiabatic Detachment Energies (ADE), Water Binding Energies (BE), and MP2 Single Point Energies of $IrCl_6^{3-}\cdot(H_2O)_n$ $n = 1-3$ Clusters

n	cluster	energy[a] (au)	rel. energy[a] (eV)	energy[b] (au)	rel. energy[b] (eV)	VDE (eV)	ADE[a] (eV)	BE (eV)
1		−270.951804		−268.675502		−3.437	−3.617	1.328
		(−270.921224)		(−268.644200)			(−3.614)	
2	I	−347.415062	0	−344.855571	0	−3.029	−3.221	1.332
		(−347.358425)	(0)	(−344.797826)	(0.029)		(−3.236)	
2	II	−347.413025	0.055	−344.855167	0.005	−2.912	−3.072	1.276
		(−347.357643)	(0.021)	(−344.798900)	(0)		(−3.090)	
2	III	−347.412423	0.072	−344.855002	0.006	−2.937	−3.148	1.260
		(−347.357165)	(0.034)	(−344.798730)	(0.005)		(−3.158)	
2	IV	−347.411660	0.093	−344.854177	0.038	−2.776	−3.138	1.239
		(−347.356371)	(0.056)	(−344.797990)	(0.025)		(−3.004)	
2	V	−347.410998	0.111	−344.854177	0.045	−2.958	−3.156	1.221
		(−347.355838)	(0.070)	(−344.798177)	(0.020)		(−3.167)	
2	VI	−347.410924	0.113	−344.853935	0.145	−2.960	−3.258	1.219
		(−347.355557)	(0.078)	(−344.797738)	(0.032)		(−3.226)	
3	I	−423.875990	0	−421.033775	0	−2.514	−2.761	−1.379
		(−423.793559)	(0)	(−420.950050)	(0.023)		(−2.781)	
3	II	−423.873940	0.056	−421.033540	0.006	−2.549	−2.817	−1.216
		(−423.792631)	(0.025)	(−420.950891)	(0)		(−2.776)	
3	III	−423.873429	0.070	−421.028649	0.139	−2.640	−2.868	−1.199
		(−423.792218)	(0.037)	(−420.946180)	(0.128)		(−2.857)	
3	IV	−423.871549	0.121	−421.032755	0.028	−2.362	−2.582	−1.203
		(−423.791535)	(0.055)	(−420.950287)	(0.016)		(−2.610)	
3	V	−423.869801	0.168	−421.025747	0.218	−2.816	−2.976	
		(−423.786712)	(0.186)	(−420.941030)	(0.268)		(−2.967)	
3	VI	−423.869726	0.170	−421.027382	0.174	−2.608	−2.846	−1.098
		(−423.787899)	(0.154)	(−420.944139)	(0.184)		(−2.848)	
3	VII	−423.867194	0.239	−421.028076	0.155	−2.650	−2.853	−1.029
		(−423.786124)	(0.203)	(−420.945508)	(0.146)		(−2.859)	
3	VIII	−423.847527	0.775	−421.004019	0.810	−2.923	−3.582	
		(−423.765315)	(0.769)	(−420.920636)	(0.823)		(−3.631)	

[a] Zero point energy corrected values are included in parentheses. [b] MP2 single point energies of B3LYP/LANL2DZ optimized structure. Zero point energy corrected values are included in parentheses.

TABLE 3: Selected Bond Lengths and Bond Angles for the Optimized $IrCl_6^{3-}\cdot(H_2O)_n$ $n = 1$ and $n = 2$ Clusters, with Bond Lengths in Angstroms and Bond Angles in Degrees

$n = 1$		$n = 2$											
		I		II		III		IV		V		VI	
H_9-Cl_2	2.31	H_9-Cl_2	2.21	H_9-Cl_2	2.32	H_9-Cl_2	2.32	H_9-Cl_2	2.31	H_9-Cl_2	2.36	H_9-Cl_2	2.17
$H_9-O_8-H_{10}$	101.2	$H_{12}-Cl_4$	2.46	$H_{13}-Cl_6$	2.32	$H_9-O_8-H_{10}$	101.4	$H_{10}-Cl_3$	2.35	$H_{10}-Cl_3$	2.31	$H_{12}-O_8$	1.56
		$H_{13}-O_8$	1.78	$H_9-O_8-H_{10}$	101.4			$H_9-O_8-H_{10}$	101.7	$H_9-O_8-H_{10}$	101.8	$H_9-O_8-H_{10}$	102.0
		$H_9-O_8-H_{10}$	101.8	$H_{12}-O_{11}-H_{13}$	101.4							$H_{12}-O_{11}-H_{13}$	105.6
		$H_{12}-O_{11}-H_{13}$	104.2										

hydrogen bond with the second water molecule (motif b). The stability of this cluster is reflected in the lengths of the bifurcated hydrogen bonds, which are reduced by 0.1 Å compared to the monohydrate, indicating that the second water molecule is acting to enhance the binding of the bifurcated water. The global minimum structure contrasts with those observed for dianion−water clusters, for example, $CO_2-(CH_2)_4-CO_2^{2-}\cdot(H_2O)_2$ in which both waters participate in bifurcated hydrogen bonds.[17] We note, however, that the type of structure observed here would not be possible for some of the more compact dianions that have been studied previously.[14−20]

Cluster II lies just 0.055 eV higher in energy than cluster I and consists of a structure in which each of the water molecules adopts a bifurcated hydrogen bond (motif a) across two sides of the $IrCl_6^{3-}$ ion. The hydrogen bonds are 0.01 Å longer than those in the monohydrate, reflecting the generally lower binding energy of a water molecule in the $n = 2$ cluster. Clusters III−V represent variations of the Cluster II structure with the water molecules adopting bifurcated hydrogen bonds, lying 0.072, 0.093, and 0.111 eV, respectively, above the global minimum. The water molecules in these structures are spatially closer than those in cluster II, leading to the slightly higher relative energies observed. Cluster VI, the highest energy isomer, contains one bifurcated water molecule, which acts as an acceptor to form a single hydrogen bond with the second water molecule. The ion−water bond lengths for the bifurcated water in cluster VI are 0.15 Å shorter than those for the monohydrate, possibly because of polarization of the bifurcated water by the second water. A similar high energy isomer was observed for the $CO_2-(CH_2)_4-CO_2^{2-}\cdot(H_2O)_2$ system.[17]

Upon inclusion of zero-point energies, the relative ordering of the isomers remains unchanged, although Cluster I displays a larger ZPE correction than the other isomers. We note that the relative ordering of the isomers may change at a higher level of theory or with a larger basis set. To provide a comparison with the DFT results, we obtained MP2 single point energies (Table 2) for the $IrCl_6^{3-}\cdot(H_2O)_2$ cluster isomers. At the MP2 level (ZPE corrected) there is some reordering of the relative energies, with cluster II becoming the global minimum and clusters III and I now lying 0.005 and 0.029 eV above the global minimum, respectively. These results suggest that the B3LYP functional may overestimate the strength of the water−water interactions within the $IrCl_6^{3-}\cdot(H_2O)_2$ clusters and provides an

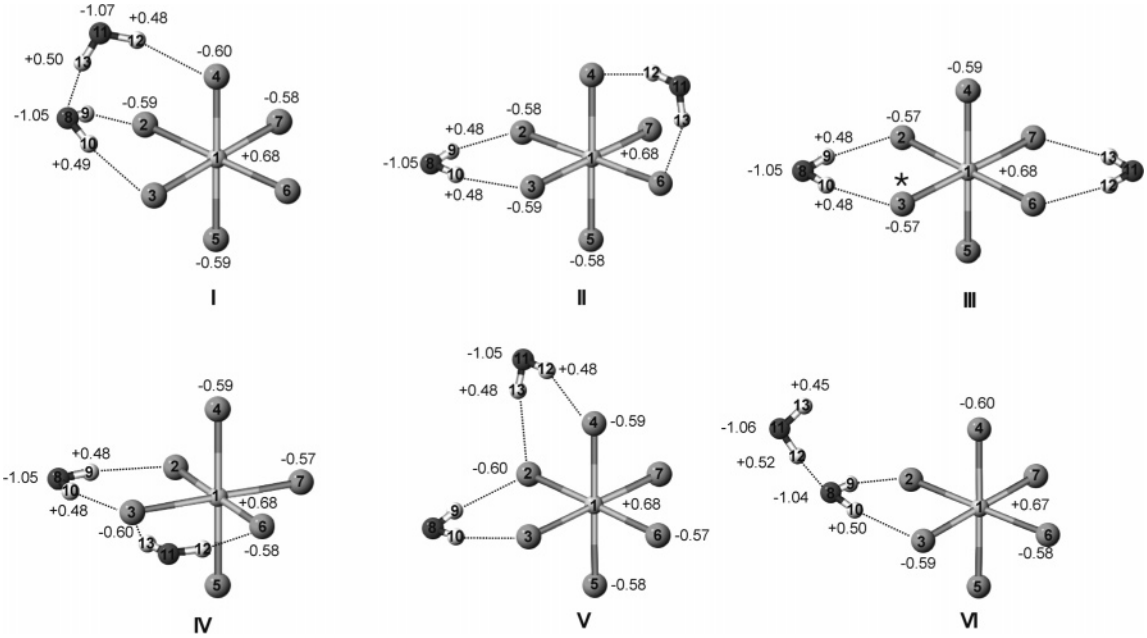

Figure 5. Geometric structures of isomers I−VI of $IrCl_6^{3-}\cdot(H_2O)_2$ obtained at the B3LYP/LANL2DZ level, displayed with NPA charges. Atom labels are in bold. The asterisk on isomer III represents the Ir−Cl bond scanned for the potential surface shown in Figure 8.

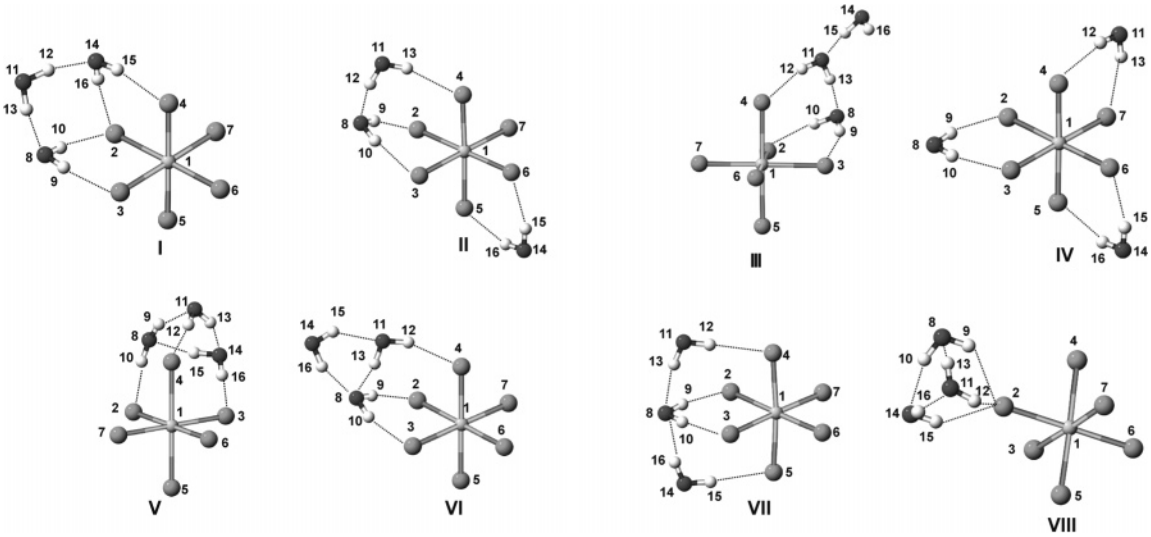

Figure 6. Geometric structures of isomers I−VIII of $IrCl_6^{3-}\cdot(H_2O)_3$ cluster obtained at the B3LYP/LANL2DZ level, with atom labels displayed in bold.

overall picture of a system in which a number of structural isomers would exist at ambient temperatures.

(iii) n = 3. Figure 6 displays eight stable minima of the $IrCl_6^{3-}\cdot(H_2O)_3$ cluster. These isomeric structures were selected for optimization because they represent the most stable form of a particular type of binding arrangement. Table 2 displays the absolute energies, MP2 single point energies, water binding energies, VDEs, and ADEs, with geometric parameters displayed in Table 4. The global minimum structure, cluster I, has two water molecules that adopt bifurcated hydrogen bonds adjacent to one another, with the third water forming a bridge between them. The geometric parameters reflect the stability of this isomer, and the hydrogen bond lengths of the bifurcated waters are shorter compared to the related $n = 2$ cluster, V. The global minimum structure again contrasts with the calculated global minima of $SO_4^{2-}\cdot(H_2O)_3$ and $C_2O_4^{2-}\cdot(H_2O)_3$ where the solvents adopt bifurcated hydrogen bonds to the ion rather than water−water bonds.[15,16]

Cluster II lies 0.056 eV above the global minimum and displays a similar structure to the $n = 2$ cluster, I (motif b), with an additional bifurcated water molecule. Cluster III is related to the $n = 2$ cluster, I, with a third water molecule bound via a single hydrogen bond to the second water molecule. As with the similar binding arrangement present for the $IrCl_6^{3-}\cdot(H_2O)_2$ VI cluster, the ion−water hydrogen bonds are significantly reduced in length. Cluster IV represents the lowest energy isomer in which all three waters adopt bifurcated hydrogen bonds. This represents the only arrangement for the $IrCl_6^{3-}\cdot(H_2O)_3$ system in which all six chlorines are in contact with the solvent. The chlorine−water bond lengths are 0.01 Å longer than those in the case of the related $n = 2$ analogue (cluster II, Figure 5) because the negative charge on the binding sites decreases with the addition of each solvent. Clusters V−VIII represent higher energy structures, which will not be discussed in detail here but are included for comparison with clusters I−IV.

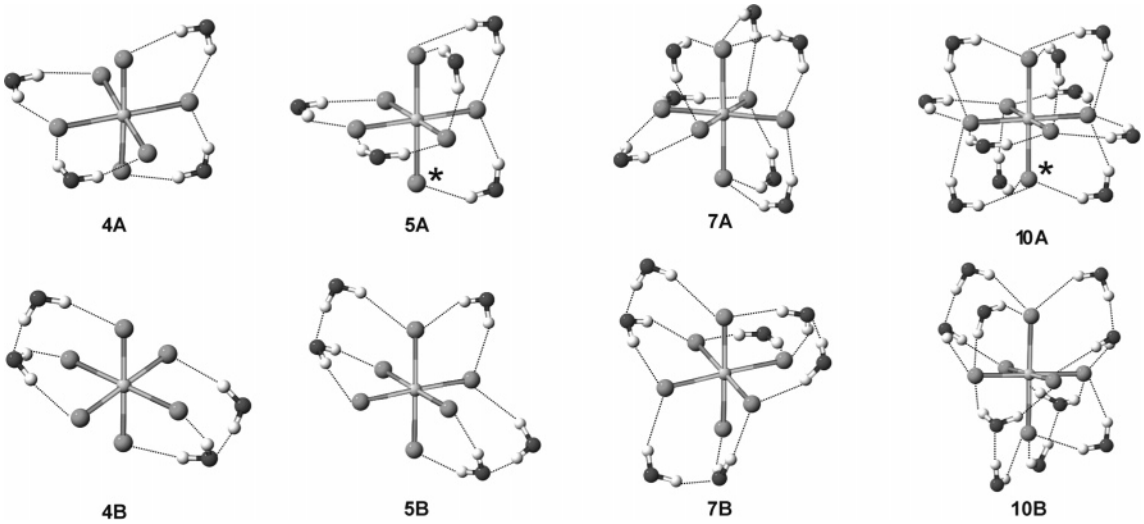

Figure 7. Geometric structures of isomers A and B of the $IrCl_6^{3-}\cdot(H_2O)_n$ $n = 4$, 5, 7, 10 clusters obtained at the B3LYP/LANL2DZ level. The asterisks represent the Ir−Cl bond scanned for the potential surfaces shown in Figure 8.

TABLE 4: Selected Bond Lengths and Bond Angles for the Optimized $IrCl_6^{3-}\cdot(H_2O)_3$ Clusters, with Bond Lengths in Angstroms and Bond Angles in Degrees

I		II		III		IV	
H_9-Cl_2	2.29	H_9-Cl_2	2.23	H_9-Cl_2	2.17	H_9-Cl_2	2.33
$H_{10}-Cl_3$	2.24	$H_{10}-Cl_3$	2.22	$H_{13}-O_8$	1.64	$H_{10}-Cl_3$	2.33
$H_{13}-O_8$	1.83	$H_{13}-O_8$	1.78	$H_{12}-Cl_4$	2.28	$H_9-O_8-H_{10}$	101.7
$H_9-O_8-H_{10}$	102.2	$H_{12}-Cl_4$	2.48	$H_{15}-O_{11}$	1.54		
$H_{12}-O_{11}-H_{13}$	105.3	$H_{15}-Cl_6$	2.33	$H_9-O_8-H_{10}$	101.9		
		$H_{16}-Cl_5$	2.33	$H_{12}-O_{11}-H_{13}$	105.1		
		$H_9-O_8-H_{10}$	102.0	$H_{15}-O_{14}-H_{16}$	106.0		
		$H_{12}-O_{11}-H_{13}$	104.5				
		$H_{15}-O_{14}-H_{16}$	101.7				
V		VI		VII		VIII	
$H_{10}-Cl_2$	2.20	H_9-Cl_2	2.16	H_9-Cl_2	2.42	H_9-Cl_2	2.39
H_9-O_{14}	1.86	$H_{13}-O_8$	1.83	$H_{13}-O_8$	2.11	$H_{10}-O_{14}$	1.94
$H_9-O_8-H_{10}$	107.9	$H_{12}-O_4$	2.31	$H_{12}-Cl_4$	2.45	$H_9-O_8-H_{10}$	105.1
		$H_{15}-O_{11}$	2.01	$H_9-O_8-H_{10}$	103.0		
		$H_{16}-O_8$	1.86	$H_{12}-O_{11}-H_{13}$	106.8		

The inclusion of ZPE corrections again results in a general decrease of the relative energies of the higher clusters relative to cluster I. As in the $n = 2$ clusters, isomers with a larger number of water−water hydrogen bonds possess a relatively large ZPE. The single point MP2 energies alter the relative ordering of the isomers significantly and again suggest that B3LYP overestimates the water−water interaction. At the MP2/LANL2DZ level (ZPE corrected), cluster II becomes the global minimum, with cluster III becoming considerably less stable, in line with the related $n = 2$ cluster, VI. The relative energies of clusters V−VIII remain substantially higher in energy than clusters I, II, and IV at the MP2 level.

(iv) n = 4−10 Clusters. For $IrCl_6^{3-}\cdot(H_2O)_4$ and the higher clusters, two sets of representative cluster structures were generated based on the lowest energy binding motifs that were identified for the $n = 3$ clusters, that is, structures in which the water molecules adopt only bifurcated hydrogen bonds to the trianion (Series A) and structures in which the water molecules adopt the maximum number of motif-b-type binding positions (Series B). The optimized cluster structures obtained for the $n = 4$, 5, 7, and 10 clusters are displayed in Figure 7, with the absolute energies, VDEs, and ADEs for the $n = 4-10$ clusters presented in Table 5. The geometric parameters are available on request. We note that the Series B isomers are more stable than the respective Series A isomers, at both the B3LYP and MP2 levels, although the relative energies are closer at the MP2 level.

(v) Summary and Further Remarks on the Cluster Structures. In summary, the DFT calculations of the $IrCl_6^{3-}\cdot(H_2O)_n$ $n = 2-10$ clusters indicate that a large number of isomeric minima are possible. Comparing the $IrCl_6^{3-}\cdot(H_2O)_n$ structures with those obtained for other hydrated dianions,[14−20] the propensity of the trianion clusters to adopt structures containing water−water bonds is striking. The stability of these motif b structures can be attributed primarily to the long Ir−Cl bond lengths (∼2.5Å) providing an optimum geometry to support water−water binding to the complex anion. Recent work on $SO_4^{2-}\cdot(H_2O)_n$ ($n = 6-12$) clusters predicted similar structures in which each water molecule forms one hydrogen bond to the ion and a second to an adjacent solvent unit.[45]

There is now a large body of experimental and theoretical work on the hydration of monoanions,[33−39] with halide ion−water clusters having been particularly intensively investigated.[33,36,37] Focusing on the microhydration of Cl^-,[33,36,37] the ion is known to bind one water molecule via a single hydrogen bond, leaving one of the water OH groups unbound. This solvation motif is reflected in the minimum energy structures of the higher clusters, for example, $Cl^-\cdot(H_2O)_n$ $n = 2-4$, in

TABLE 5: B3LYP/LANL2DZ Absolute Energies, Vertical Detachment Energies (VDE), Adiabatic Detachment Energies (ADE), Water Binding Energies (BE), and MP2 Single Point Energies of $IrCl_6^{3-}\cdot(H_2O)_n$ $n = 4-10$

n	cluster	energy[a] (au)	rel. energy[a] (eV)	energy[b] (au)	rel. energy[b] (eV)	VDE (eV)	ADE[a] (eV)	BE (eV)
4	A	−500.325440	0.218	−497.206674	0.100	−1.898	−2.113	1.077
		(−500.221109)	(0.139)	(−497.101031)	(0.011)			
4	B	−500.333443	0	−497.210338	0	−2.163	−2.381	1.230
		(−500.226235)	(0)	(−497.101394)	(0.001)			
5	A	−576.776236	0.276	−573.378115	0.133	−1.570	−1.793	0.993
		(−576.647750)	(0.192)	(−573.248131)	(0.038)			
5	B	−576.786372	0	−573.382992	0	−1.722	−1.939	1.051
		(−576.654794)	(0)	(−573.249543)	(0)			
6	A	−653.225434	0.470	−649.547670	0.313	−1.202	−1.356	0.949
		(−653.072838)	(0.337)	(−649.393546)	(0.181)			
6	B	−653.242734	0	−649.559177	0	−1.374	−1.1612	1.144
		(−653.085221)	(0)	(−649.400190)	(0)			
7	A	−729.670371	0.587	−725.713343	0.376	−0.741	−1.070	0.833
		(−729.494209)	(0.438)	(−725.535593)	(0.210)			
7	B	−729.691935	0	−725.727144	0	−0.901	−1.232	0.949
		(−729.510302)	(0)	(−725.543294)				
8	A	−806.113353	0.819	−801.876502	0.567	−0.490	−0.613	0.780
		(−805.913564)	(0.609)	(−801.675517)	(0.330)			
8	B	−806.143482	0	−801.897330	0	−0.693	−0.995	1.013
		(−805.935949)	(0)	(−801.687653)	(0)			
9	A	−882.554431	0.857	−878.038299	0.607	−0.087	−0.327	0.725
		(−882.331007)	(0.645)	(−877.144058)	(0.356)			
9	B	−882.585793	0	−878.060587	0	−0.388	−0.693	0.762
		(−882.354706)	(0)	(−877.827494)	(0)			
10	A	−958.993332	0.971	−954.196336	0.661	0.263	0.009	0.672
		(−958.739859)	(0.971)	(−953.949364)	(0.416)			
10	B	−959.026803	0	−954.196336	0	−0.007	−0.473	0.726
		(−958.772287)	(0)	(−953.964593)	(0)			

[a] Zero point energy corrected values are included in parentheses. [b] MP2 single point energies of B3LYP/LANL2DZ optimized structure.

which the water molecules bind to the halide via single donor hydrogen bonds with the second water OH group engaging in water−water hydrogen bonding. Comparing the structures of the $Cl^-\cdot(H_2O)n$ clusters with the $IrCl_6^{3-}\cdot(H_2O)_n$ clusters studied here, we note that the water molecules in the $IrCl_6^{3-}\cdot(H_2O)_n$ systems display at least one bifurcated hydrogen bond in each structure. We note that this observation could be attributed partially to the reduced partial charge (i.e., <1e) on the Cl^- ligands in $IrCl_6^{3-}$ but is more straightforwardly a result of the multiple Cl^- ligands present in the complex anion. It is instructive to consider the results of a recent study of $Cl_2^-\cdot(H_2O)_n$ clusters in this context[35] because the evenly distributed charge within Cl_2^- is solvated via bifurcated hydrogen bonds in the $n = 1$ and 2 clusters.

D. The Effect of Microsolvation on the Stability of $IrCl_6^{3-}$ with Respect to Electron Detachment and Ionic Fragmentation. A number of previous studies have established that both monoanions and dianions are stabilized with respect to electron detachment with an increase in the degree of solvation.[14−18,46,47] The VDE and ADE results presented for the $IrCl_6^{3-}\cdot(H_2O)_n$ $n = 1-10$ clusters in Section 4C illustrate that the same trend operates for the trianionic system studied here. For the series A clusters, the ADE is just positive at $n = 10$, indicating that $IrCl_6^{3-}\cdot(H_2O)_{10}$ is the first cluster adopting this geometric structure to be electronically stable. Extrapolation of the ADE values for the series B clusters indicates that $IrCl_6^{3-}\cdot(H_2O)_{12}$ would typically be the first electronically stable cluster within this class. In practice, $IrCl_6^{3-}\cdot(H_2O)_n$ clusters would be produced using electrospray ionization, where a thermal distribution of clusters of different structural types would be expected under typical operating conditions. This leads us to predict that the onset for observing $IrCl_6^{3-}\cdot(H_2O)_n$ clusters would occur at $n = 10-11$. This result can be compared with related dianionic systems where the isolated dianion is electronically unstable. For example, unsolvated SO_4^{2-} is electronically unstable, whereas $SO_4^{2-}\cdot(H_2O)_3$ can be observed experimentally,[15,19,20] and four water molecules are needed to stabilize $C_2O_4^{2-}$.[16]

Figure 8 presents 1D potential energy scans for ionic fragmentation of the $IrCl_6^{3-}\cdot(H_2O)_n$ $n = 1$, 2, 5, 10 (Series A) clusters. For all of the scans, as the Ir−Cl bond extends, the adjacent H_2O is observed to leave with the Cl^-. Figure 8a displays three scans for $IrCl_6^{3-}\cdot H_2O$, obtained along each of the three distinctive Ir−Cl bond axes of the complex. The scans reveal very similar fragmentation surfaces for the unsolvated axial and equatorial Ir−Cl bonds (pathways 1 and 2), whereas the surface for removal of the solvated Cl^- ion (pathway 3) lies ∼0.2 eV lower. Figure 8b compares the potential energy scans for the $n = 1$, 2, 5, 10 clusters. The scans clearly illustrate that the RCB_{if}(inner) increases with increasing solvation, whereas the RCB_{if}(outer) decreases, revealing that the $IrCl_6^{3-}$ trianion is stabilized with respect to ionic fragmentation with increasing solvation.

The potential energy scans in Figure 8 exclusively explore fragmentation of the $IrCl_6^{3-}$ core trianion into the $IrCl_5^{2-}$ and Cl^- moieties. However, an alternative pathway for ionic fragmentation for these clusters could exist involving proton transfer from a water molecule, with subsequent loss of OH^-. Indeed, this type of decay pathway has been observed previously for a number of systems involving hydrated protic dianions, such as SO_4^{2-}.[20] Analogous barrierless decay pathways have also been observed for highly charged cationic systems, including the solvated Zr^{4+} clusters discussed in the Introduction.[13] We saw no evidence for this type of decay processes in our systems. A search for a proton-transfer path in the $IrCl_6^{3-}\cdot(H_2O)$

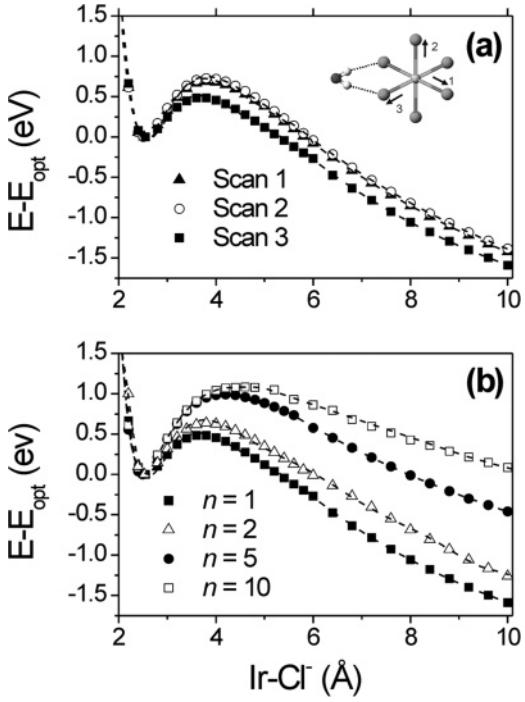

Figure 8. Calculated potential energy curves for ionic fragmentation of $IrCl_6^{3-}\cdot(H_2O)_n$ clusters. (a) Scans for the $n = 1$ cluster along the Ir−Cl bonds indicated. (b) Scans for the $n = 1$, 2, 5, 10 clusters. The scan for $n = 1$ displayed corresponds to Scan 3 in (a). The scans for the $n = 2$, 5, 10 clusters correspond to scanning the Ir−Cl bonds of the isomer marked with an asterisk in Figures 5 and 7.

cluster revealed that the energy of the cluster dramatically increases as an OH^- group is scanned away from the equilibrium structure. To investigate whether the proton-transfer propensity increased with the onset of a second solvation shell (as in $Zr^{4+}\cdot(H_2O)_n$), calculations were performed on $IrCl_6^{3-}\cdot(H_2O)_{13}$, where the 13th H_2O was positioned in the second shell. However, in contrast to the Zr^{4+} clusters, spontaneous decay via proton transfer does not occur. It appears that unlike the covalent dianions discussed earlier the proton affinity of $IrCl_6^{3-}$ is insufficient to overcome the strength of the O−H water bond.

4. Concluding Remarks

The calculations on $IrCl_6^{3-}$ presented above show that the unsolvated trianion is unstable with respect to electron detachment because of rapid electron tunneling through the repulsive coulomb barrier. $IrCl_6^{3-}$ is also predicted to be more unstable with respect to ionic fragmentation compared to $IrCl_6^{2-}$. Although the bare $IrCl_6^{3-}$ ion is intrinsically unstable in the gas phase, it is known to be a stable complex anion in a condensed phase environment. Our calculations demonstrate that $IrCl_6^{3-}$ becomes stable with respect to both electron detachment and ionic fragmentation with sequential solvation. Focusing on ionic fragmentation, RCB_{if}(inner) gradually increases with solvation, whereas RCB_{if}(outer) decreases. We anticipate that this behavior will be generic for the prototypical aprotic MCA studied here.

We have recently discussed the factors that control the RCBs for ionic fragmentation in an experimental study of ionic fragmentation versus electron detachment in isolated transition-metal complex dianions (i.e., MX_6^{2-}, where M = Ir, Os, Re and X = Cl, Br).[8] The outer RCB was found to be associated with the intramolecular Coulomb repulsion, whereas the magnitude of the inner RCB was observed to reflect the purely attractive binding energy of an X^- ion to an MX_5^- moiety, that is, $\Delta E(MX_5^- + X^-)$ − intramolecular Coulomb repulsion. Applying this model, RCB_{if}(outer) reduces with increasing solvation because of the reduction in the intramolecular Coulomb repulsion that arises from the increased dielectric shielding of the excess negative charges provided by increasing numbers of solvent molecules. For RCB_{if}(inner), increasing solvation increases the magnitude of the RCB because each additional water molecule generates an additional exothermic ion−water interaction.

The potential energy scans of the $IrCl_6^{3-}\cdot H_2O$ cluster presented in Figure 8a reveal the asymmetry of the surfaces for ionic fragmentation and illustrate that the RCB_{if}(inner) for fragmentation of an Ir−Cl bond in which the Cl is directly solvated by a water molecule (scan 3) is lower than fragmentation along an unsolvated Ir−Cl bond (scans 1 and 2). Our model (ref 8) indicates that this arises because of a lower attractive binding energy along the scan 3 coordinate, presumably because of the fact that a single Cl^- ion will bind more strongly to a water molecule than an $IrCl_5^{2-}$ complex anion.

It is instructive to compare the results obtained in this work with recent results from Harvey and Kaczowska on highly charged cations.[13] For the solvated tetracations studied, all of the systems were thermodynamically unstable, that is, one or more charge-separated dissociation asymptotes lie lower in energy than the solvated cation minimum. This does not mean that the cations will spontaneously dissociate, however, because the solvated ions can display substantial metastable lifetimes because of the presence of the RCB on the potential energy surface. We note that this behavior is different from that of the highly charged anionic systems studied here because the metastable triply charged anions are able to decay *despite* the presence of the RCB because of spontaneous electron tunneling. On this basis, highly charged MCAs can be considered to be intrinsically less stable than highly charged multiply charged cations.

Although our results indicate that the direct experimental observation of $IrCl_6^{3-}$ will prove to be experimentally challenging, it should be possible to observe hydrated clusters of the trianion, such as $IrCl_6^{3-}\cdot(H_2O)_{12}$, using electrospray ionization mass spectrometry techniques. Several groups have employed this approach and observed hydrated clusters of molecular dianions that are electronically unstable as isolated gas-phase anions.[14−16,19,20] A robust example is provided by SO_4^{2-}, where $SO_4^{2-}\cdot(H_2O)_n$ clusters with $n \geq 3$ have been experimentally observed in line with the calculated onset of electronic stability.[15,19,20] Other approaches to the dissolution process are available,[48,49] and could be adapted to provide additional insight into the bulk solvation of ions such as $IrCl_6^{3-}$. Finally, we note that it may be possible to transiently observe $IrCl_6^{3-}$ or its daughter ions via high-energy collision of an electron donor species such as Na with $IrCl_6^{2-}$.[9] Experimental efforts toward this end are currently underway in this group.

Acknowledgment. C.E.H.D. thanks the Royal Society for support from a University Research Fellowship and the Leverhulme Trust for support through grant F00224K.

References and Notes

(1) Wang, L. S. *Comments Mod. Phys.* **2001**, *2*, 207−221.
(2) Scheller, M. K.; Compton, R. N.; Cederbaum, L. S. *Science* **1995**, *270*, 1160−1166.
(3) Dreuw, A.; Cederbaum, L. S. *Chem. Rev.* **2002**, *102*, 181−200.
(4) Schröder, D. *Angew. Chem., Int. Ed.* **2004**, *43*, 1329−1333.
(5) Boldyrev, A. I.; Gutowski, M.; Simons, J. *Acc. Chem. Res.* **1996**, *29*, 497−502.

(6) Compton, R. N.; Tuinman, A. A.; Klots, C. E. *Phys. Rev. Lett.* **1997**, *78*, 4367−4370.
(7) Blom, M. N.; Hampe, O.; Gilb, S.; Weis, P.; Kappes, M. M. *J. Chem. Phys.* **2001**, *115*, 3690−3697.
(8) Boxford, W. E.; Pearce, J. K.; Dessent, C. E. H. *Chem. Phys. Lett.* **2004**, *399*, 465−470.
(9) Nielsen, A. B.; Hvelplund, P.; Liu, B.; Nielsen, S. B.; Tomita, S. *J. Am. Chem. Soc.* **2003**, *125*, 9592−9593.
(10) Stace, A. J. *J. Phys. Chem. A* **2002**, *106*, 7993−8005.
(11) Metz, R. B. *Int. J. Mass Spectrom.* **2004**, *235*, 131−143.
(12) Beyer, M.; Williams, E. R.; Bondybey, V. E. *J. Am. Chem. Soc* **1999**, *121*, 1565−1573.
(13) Harvey, J. N.; Kaczorowska, M. *Int. J. Mass Spectrom.* **2003**, *228*, 517−526.
(14) Ding, C. F.; Wang, X. B.; Wang, L. S. *J. Phys. Chem. A* **1998**, *102*, 8633−8636.
(15) Yang, X.; Wang, X. B.; Wang, L. S. *J. Phys. Chem. A* **2002**, *106*, 7607−7616.
(16) Wang, X. B.; Yang, X.; Nicholas, J. B.; Wang, L. S. *J. Chem. Phys.* **2003**, *119*, 3631−3640.
(17) Dessent, C. E. H.; Rigby, C. *Chem. Phys. Lett.* **2003**, *370*, 52−61.
(18) Kambalapalli, S.; Ortiz, J. V. *J. Phys. Chem. A* **2003**, *107*, 10360−10369.
(19) Blades, A. T.; Kebarle, P. *J. Am. Chem. Soc.* **1994**, *116*, 10761−10766.
(20) Wong, R. L.; Williams, E. R. *J. Phys. Chem. A* **2003**, *107*, 10976−10983.
(21) Stefanovich, E. V.; Boldyrev, A. I.; Truong, T. N.; Simons, J. *J. Phys. Chem. B* **1998**, *102*, 4205−4208.
(22) Dreuw, A.; Cederbaum, L. S. *J. Chem. Phys.* **2000**, *112*, 7400−7408.
(23) Wang, X. B.; Wang, L. S. *J. Chem. Phys.* **1999**, *111*, 4497−4509.
(24) Friedrich, J.; Gilb, S.; Ehrler, O. T.; Behrendt, A.; Kappes, M. M. *J. Chem. Phys.* **2002**, *117*, 2635−2644.
(25) Greenwood, N. N.; Earnshaw, A. *Chemistry of the Elements*; Pergamon: Oxford, U.K., 1984.
(26) Watkins, J. J.; White, H. S. *Langmuir* **2004**, *20*, 5474−5483.
(27) Becke, A. D. *J. Chem. Phys.* **1993**, *98*, 5648−5652.
(28) Hay, P. J.; Wadt, W. R. *J. Chem. Phys.* **1985**, *82*, 299−310.
(29) Frisch, M. J.; Trucks, G. W.; Schlegel, H. B.; Scuseria, G. E.; Robb, M. A.; Cheeseman, J. R.; Montgomery, Jr., J. A.; Vreven, T.; Kudin, K. N.; Burant, J. C.; Millam, J. M.; Iyengar, S. S.; Tomasi, J.; Barone, V.; Mennucci, B.; Cossi, M.; Scalmani, G.; Rega, N.; Petersson, G. A.; Nakatsuji, H.; Hada, M.; Ehara, M.; Toyota, K.; Fukuda, R.; Hasegawa, J.; Ishida, M.; Nakajima, T.; Honda, Y.; Kitao, O.; Nakai, H.; Klene, M.; Li, X.; Knox, J. E.; Hratchian, H. P.; Cross, J. B.; Bakken, V.; Adamo, C.; Jaramillo, J.; Gomperts, R.; Stratmann, R. E.; Yazyev, O.; Austin, A. J.; Cammi, R.; Pomelli, C.; Ochterski, J. W.; Ayala, P. Y.; Morokuma, K.; Voth, G. A.; Salvador, P.; Dannenberg, J. J.; Zakrzewski, V. G.; Dapprich, S.; Daniels, A. D.; Strain, M. C.; Farkas, O.; Malick, D. K.; Rabuck, A. D.; Raghavachari, K.; Foresman, J. B.; Ortiz, J. V.; Cui, Q.; Baboul, A. G.; Clifford, S.; Cioslowski, J.; Stefanov, B. B.; Liu, G.; Liashenko, A.; Piskorz, P.; Komaromi, I.; Martin, R. L.; Fox, D. J.; Keith, T.; Al-Laham, M. A.; Peng, C. Y.; Nanayakkara, A.; Challacombe, M.; Gill, P. M. W.; Johnson, B.; Chen, W.; Wong, M. W.; Gonzalez, C.; Pople, J. A. *Gaussian 03*, Revision C.02; Gaussian, Inc., Wallingford CT, 2004.
(30) Reed, A. E.; Weinstock, R. B.; Weinhold, F. A. *J. Chem. Phys.* **1985**, *83*, 735−746.
(31) Hall, R. J.; Hillier, I. H.; Vincent, M. A. *Chem. Phys. Lett.* **2000**, *320*, 139−143.
(32) Pan, Y. P.; McAllister, M. A. *J. Am Chem. Soc.* **1997**, *119*, 7561−7566.
(33) Roberston, W. H.; Johnson, M. A. *Annu. Rev. Phys. Chem.* **2003**, *54*, 173-213; and references therein.
(34) Weber, J. M.; Kelley, J. A.; Nielsen, S. B.; Ayotte, P.; Johnson, M. A. *Science* **2004**, *287*, 2461−2463.
(35) Price, E. A.; Hammer, N. I.; Johnson, M. A. *J. Phys. Chem. A.* **2004**, *108*, 3910−3915.
(36) Kim, J.; Lee, H. M.; Suh, S. B.; Majumdar, D.; Kim, K. S. *J. Chem. Phys.* **2000**, *113*, 5259−5272.
(37) Xantheas, S. S. *J. Phys. Chem.* **1996**, *100*, 9703−9713.
(38) Bell, A. J.; Wright, T. G. *Phys. Chem. Chem. Phys.* **2004**, *6*, 4385−4390.
(39) Robertson, W. H.; Karapetian, K.; Ayotte, P.; Jordan, K. D.; Johnson, M. A. *J. Chem. Phys.* **2002**, *116*, 4853−4857.
(40) Jenkins, H. D. B.; Pratt, K. F. *Adv. Inorg. Chem. Radiochem.* **1979**, *22*, 1−111.
(41) Deeth, R. J.; Jenkins, H. D. B. *J. Phys. Chem. A.* **1997**, *101*, 4793−4798.
(42) Simons, J.; Skurski, P.; Barrios, R. *J. Am. Chem. Soc.* **2000**, *122*, 11893−11899.
(43) Shi, Q.; Kais, S. *J. Am. Chem. Soc.* **2002**, *124*, 11723−11729.
(44) Dreuw, A.; Cederbaum, L. S. *J. Phys. Chem. A* **2001**, *105*, 10577−10582.
(45) Gao, B.; Liu, Z. *J. Chem. Phys.* **2004**, *121*, 8299−8306.
(46) Markovich, G.; Pollack, S.; Giniger, R.; Cheshnovsky, O. *J. Chem. Phys.* **1994**, *101*, 9344−9353.
(47) Coe, J. V.; Lee, G. H.; Eaton, J. G.; Arnold, S. T.; Sarkas, H. W.; Ludewight, C.; Haberland, H.; Worsnop, D. R.; Bowen, K. H. *J. Chem. Phys.* **1990**, *92*, 3980−3982.
(48) Ostrovskii, V. E.; Tsurkova, B. V.; Kadyshevich, E. A.; Gostev, B. V. *J. Phys. Chem. B* **2001**, *105*, 12680−12687.
(49) Ostrovskii, V. E.; Kadyshevich, E. A. *Int. J. Nanosci.* **2002**, *1*, 101−121.